Chebyshev-type rational approximations of the one-way Helmholtz equation for solving a class of wave propagation problems

Mikhail S. Lytaev[0000−0001−7082−4716]

St. Petersburg Federal Research Center of the Russian Academy of Sciences, 14-th Linia, V.I., No. 39, Saint Petersburg 199178, Russia mikelytaev@gmail.com

Abstract. This study is devoted to improving the efficiency of the numerical methods for solving the pseudo-differential parabolic equation of diffraction theory. A rational approximation on an interval is used instead of the Padé approximation in a vicinity of a point. The relationship between the pseudo-differential propagation operator, variations of the refractive index, and the maximum propagation angle is established. It is shown that using the approximation on an interval is more natural for this problem and allows using a more sparse computational grid than when using the local Padé approximation. The proposed method differs from the existing ones only in the coefficients of the numerical scheme and does not require significant changes in the implementations of the existing numerical schemas. The application of the proposed approach to the tropospheric radio-wave propagation and underwater acoustics is provided. Numerical examples quantitatively demonstrate the advantages of the proposed approach.

Keywords: Wave propagation · Helmholtz equation · Parabolic equation · Diffraction · Rational approximation

1 Introduction

A wide class of wave propagation problems can be effectively tackled by the parabolic equation (PE) method [13, 6] and its wide-angle higher-order approximations. Initially, the PE method was proposed by Leontovich and Fock [12] for tropospheric radio-wave propagation problems. PE method allows handling variations of the tropospheric refractive index, irregular terrain, rough sea surface [13], vegetation [23] and backscattering [20, 30]. There are works on the application of the PE method in a substantially three-dimensional urban environment [15]. Numerical methods for solving PE have been particularly developed in computational underwater acoustics studies [7, 5, 26]. Wide-angle approximations and higher-order finite-difference numerical schemas were developed. In modern studies, the PE method is usually considered as the one-way Helmholtz equation, which is the generalization of the standard Leontovich-Fock PE [10]. This method is also widely used in geophysics [19], optics [3] and quantum mechanics [28]. The use of the principle of universality of mathematical models

ICCS Camera Ready Version 2021
To cite this paper please use the final published version:
DOI: 10.1007/978-3-030-77961-0_35

[25] promotes the mutual exchange of numerical methods for the PE between different subject areas.

The wide popularity of the PE method in the wave propagation studies is due to its strict deterministic nature and, at the same time, its high computational efficiency. Several computational programs for various purposes have been developed on the basis of the PE method: AREPS [4], PETOOL [21], RAM [24], CARPET [11]. At the same time, the problem of developing fast and reliable numerical schemas for solving PE remains relevant. Most of the works on the numerical solution of the PE are purely theoretical in nature and do not take into account the features of using these numerical algorithms in complex software systems. It is important not only to develop an efficient numerical algorithm but also to determine the limits of its applicability depending on the input data. At the same time, these algorithms should work autonomously, without an expert's intervention. Suitable artificial parameters of numerical schemas, such as the grid steps and approximation order, should be selected automatically based on the input data and the required accuracy [16].

To solve the above mentioned problems, a deep theoretical analysis of the numerical scheme is required. In this paper, we analyze the structure of the pseudo-differential propagation operator, which enables us to establish the relationship between the input parameters of the algorithm and the required approximation accuracy. This analysis allowed us to choose a more suitable approximation of the propagation operator than the existing ones.

The paper is organized as follows. The next section briefly describes the mathematical formulation of the problem. Section 3 is devoted to the development and analysis of various rational approximations of the propagation operator. Section 4 analyzes the results of numerical simulations for various propagation scenarios.

2 Problem statement

Complex wave field component $\psi(x, z)$ follows the two-dimensional Helmholtz equation

$$\frac{\partial^2 \psi}{\partial x^2} + \frac{\partial^2 \psi}{\partial z^2} + k^2 n^2(x, z)\psi = 0, \tag{1}$$

where $n(x, z)$ is the refractive index of the medium, $k = 2\pi/\lambda$ is the wavenumber, λ is the wavelength. The schematic description of the problem under consideration is shown in Fig.1. Depending on the specifics of a particular task, function ψ is subject to the impedance boundary condition [13] or transparent boundary condition [8, 27, 18] on the lower and upper boundaries of the computational domain. The wave process is generated by the initial Dirichlet condition of the form

$$\psi(0, z) = \psi_0(z)$$

ICCS Camera Ready Version 2021
To cite this paper please use the final published version:
DOI: 10.1007/978-3-030-77961-0_35

with known function $\psi_0(z)$, which corresponds to the radiation pattern of the source. Depending on the specific task, function ψ can respond to the electromagnetic field [13] or the acoustic pressure field [6].

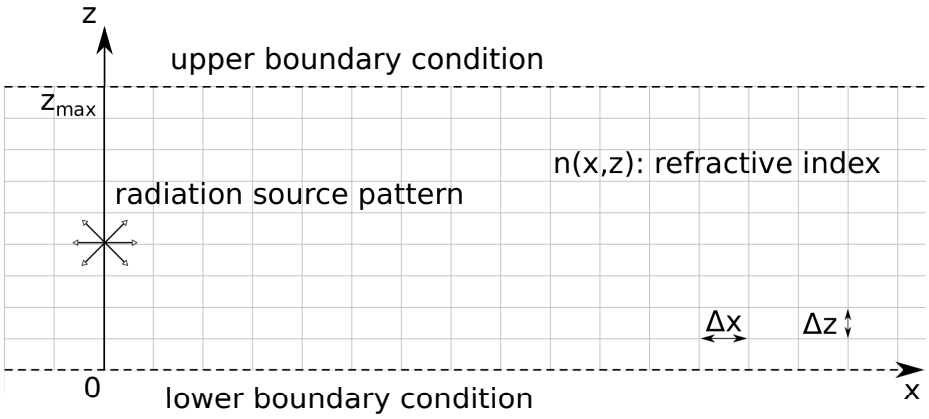

Fig. 1. Schematic description of the considered problem.

Step-by-step solution with longitudinal step Δx for the outgoing waves can be written using the pseudo-differential propagation operator as follows [13]

$$u^{n+1} = \exp\left(ik\Delta x\left(\sqrt{1+L}-1\right)\right)u^n, \tag{2}$$

where

$$u^n(z) = u(n\Delta x, z),$$

$$Lu = \frac{1}{k^2}\frac{\partial^2 u}{\partial z^2} + \left(n^2(x,z)-1\right)u,$$

$$u(x,z) = e^{-ikx}\psi(x,z). \tag{3}$$

3 Approximation of the propagator

Using the definition of a pseudo-differential operator [29], we can rewrite propagation operator (2) using the Fourier transform as follows

$$\tilde{u}^{n+1}(k_z) = \exp\left(ik\Delta x\left(\sqrt{1-\frac{k_z^2}{k^2}+(n^2(x,z)-1)}-1\right)\right)\tilde{u}^n(k_z), \tag{4}$$

ICCS Camera Ready Version 2021
To cite this paper please use the final published version:
DOI: 10.1007/978-3-030-77961-0_35

where

$$\tilde{u}^n(k_z) = \frac{1}{\sqrt{2\pi}} \int\limits_{-\infty}^{+\infty} u^n(z) e^{-ik_z z} dk_z, \tag{5}$$

$$u^n(z) = \frac{1}{\sqrt{2\pi}} \int\limits_{-\infty}^{+\infty} \tilde{u}^n(k_z) e^{ik_z z} dz. \tag{6}$$

The physical meaning of the Fourier transform (5)-(6) is the decomposition of a vertical wavefront u^n into plane waves. Vertical wavenumber k_z is related to the angle between the plane wave direction and the positive x-axis direction θ (propagation angle) as follows

$$k_z = k \sin\theta.$$

Next, we use a rational approximation of order $[n/m]$

$$\exp\left(ik\Delta x\left(\sqrt{1+\xi}-1\right)\right) \approx \frac{1+\sum_{l=1}^{m} \tilde{a}_l L^l}{1+\sum_{l=1}^{n} \tilde{b}_l L^l} = \prod_{l=1}^{p} \frac{1+a_l\xi}{1+b_l\xi}, \tag{7}$$

where

$$\xi = -\frac{k_z^2}{k^2} + \left(n^2(x,z)-1\right). \tag{8}$$

The selection of coefficients and the properties of this approximation will be clarified in the next subsections.

Taking into consideration p-1 new temporary functions $\tilde{v}_l(z)$, expression (4) can be approximately rewritten as follows

$$\begin{cases} \left(1+b_1\left(-\frac{k_z^2}{k^2}+n^2-1\right)\right)\tilde{v}_1^n = \left(1+a_1\left(-\frac{k_z^2}{k^2}+n^2-1\right)\right)\tilde{u}^{n-1} \\ \left(1+b_l\left(-\frac{k_z^2}{k^2}+n^2-1\right)\right)\tilde{v}_l^n = \left(1+a_l\left(-\frac{k_z^2}{k^2}+n^2-1\right)\right)\tilde{v}_{l-1}^n \qquad l=2\ldots p-1 \\ \ldots \\ \left(1+b_p\left(-\frac{k_z^2}{k^2}+n^2-1\right)\right)\tilde{u}^n = \left(1+a_p\left(-\frac{k_z^2}{k^2}+n^2-1\right)\right)\tilde{v}_{p-1}^n. \end{cases} \tag{9}$$

Applying the inverse Fourier transform to each line of the system (9), we obtain the following system of one-dimensional second-order differential equations

$$\begin{cases} \left(1+b_1 L\right) v_1^n = \left(1+a_1 L\right) u^{n-1} \\ \left(1+b_l L\right) v_l^n = \left(1+a_l L\right) v_{l-1}^n \qquad l=2,\ldots,p-1 \\ \ldots \\ \left(1+b_p L\right) u^n = \left(1+a_p L\right) v_{p-1}^n. \end{cases} \tag{10}$$

ICCS Camera Ready Version 2021
To cite this paper please use the final published version:
DOI: 10.1007/978-3-030-77961-0_35

System (10) can be solved sequentially from top to bottom. Next, we use the Numerov method [18] with transverse grid step Δz to approximate the second derivative. Then, each line of system (10) can be numerically solved by the tridiagonal matrix method in linear time.

Note that the overall complexity of the propagation algorithm is

$$O\left(\frac{x_{max}}{\Delta x} \cdot \frac{z_{max}}{\Delta z} \cdot p\right),$$

where x_{max} and z_{max} are longitudinal and transverse sizes of the computational domain respectively.

3.1 Padé approximation

Lets now return to the features of approximation (7). In [5] it is proposed to use the Padé approximations [2] to calculate the coefficients a_l and b_l of expansion (7). This approach is called the split-step Padé method. The basis of the Padé approximation is the expansion of the function in the vicinity of the point $\xi = 0$ according to the Taylor series. Then the coefficients of the Taylor expansion are recalculated into a_l and b_l using specially elaborated numerical methods [2]. It is important that the approximation obtained in this way is localized at a specific point ($\xi = 0$).

We introduce the absolute error of approximation of the propagation operator at each longitudinal step

$$R(\xi, a_1 \dots a_p, b_1 \dots b_p, \Delta x) = |\exp\left(ik\Delta x\left(\sqrt{1+\xi}-1\right)\right) - \frac{\prod_{l=1}^{p} 1 + a_l\xi}{\prod_{l=1}^{p} 1 + b_l\xi}|.$$

In all further examples, we consider the absolute approximation error equal to 10^{-3} to be acceptable. Note that this error refers to a single step along the longitudinal coordinate, and it accumulates during the step-by-step propagation.

To assess the quality of Padé approximation of the propagator, we consider the dependence of the absolute error of the approximation R on the value ξ for various approximation parameters shown in Fig. 2. As expected, the maximum precision of the Padé approximation is achieved near the point $\xi = 0$, monotonically decreasing as we move away from it. It is clearly seen that an increase in the order of approximation and a decrease in the step Δx lead to a more precise approximation on a larger interval.

3.2 Rational approximation on an interval

One can clearly see from expression (8) that the value of ξ is affected by the propagation angle θ and the variations of the refractive index $n(x, z)$. In the case of a homogeneous medium $\xi \in [-\sin^2\theta_{max}, 0]$, where θ_{max} is the maximum propagation angle, which can be estimated based on the geometry of a particular problem. Table 1 shows how the interval size increases depending on the maximum propagation angle.

ICCS Camera Ready Version 2021
To cite this paper please use the final published version:
DOI: 10.1007/978-3-030-77961-0_35

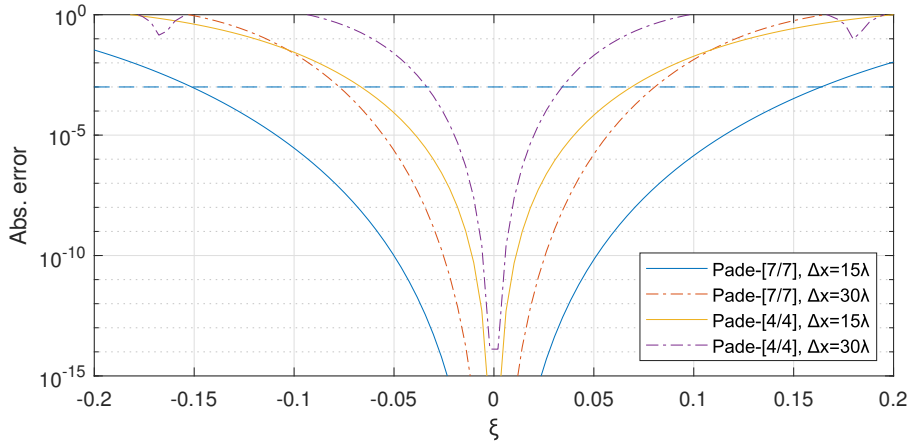

Fig. 2. Dependence of the Padé approximation error on the value ξ for various approximation orders ([4/4] and [7/7]) and longitudinal grid steps Δx (15λ and 30λ).

Table 1. The maximum propagation angle θ_{max} and the value of the interval, on which the approximation should be performed.

$\theta_{max}, ^\circ$	1	2	5	10	20	45	90
Interval $[-\sin^2\theta_{max}, 0]$	[-0.0003,0]	[-0.001,0]	[-0.008,0]	[-0.03,0]	[-0.1,0]	[-0.5,0]	[-1.0,0]

Let's assume that the values of the function $n^2(x,z)-1$ belong to the set $[t_{min}, t_{max}]$. Then $\xi \in [-\sin^2\theta_{max} + t_{min}, t_{max}]$.

Thus, we naturally come to the necessity of constructing an approximation of function (7) on the interval instead of a local approximation in the vicinity of point $\xi = 0$. Next, we consider the following two rational approximations on an interval, implemented in the Chebfun library [1]: Clenshaw-Lord method [2] (*chebpade* function in Chebfun) and the rational interpolation in the Chebyshev roots [22] (*ratinterp* function in Chebfun). Clenshaw-Lord method is based on the Chebyshev series expansion instead of the Taylor series, thus it is also known as Chebyshev-Padé method.

Fig. 3 demonstrates the dependence of the absolute approximation error R on the propagation angle θ for the Padé approximation, Clenshaw-Lord approximation, and interpolation in Chebyshev roots. In all three cases, the approximation order is [7/7], $\Delta x = 200\lambda$, so all three considered configurations are computationally equivalent. It is clearly seen that with the selected parameters, the Padé approximation can provide the required accuracy only for propagation angles up to 6°. Approximation on the interval, in turn, allows one to take into account the propagation angles up to 10° with the same approximation order and the value of Δx. The local nature of the Padé approximation is clearly observable. Namely, it has excessive accuracy at small propagation angles, while the accuracy monotonically decreases with increasing propagation angle. The error of the

ICCS Camera Ready Version 2021
To cite this paper please use the final published version:
DOI: 10.1007/978-3-030-77961-0_35

Clenshaw-Lord approximation and interpolation in Chebyshev nodes does not exceed the threshold for the entire interval $[0; 10°]$. At the same time, the latter gives slightly better accuracy, so we will use it in all further examples.

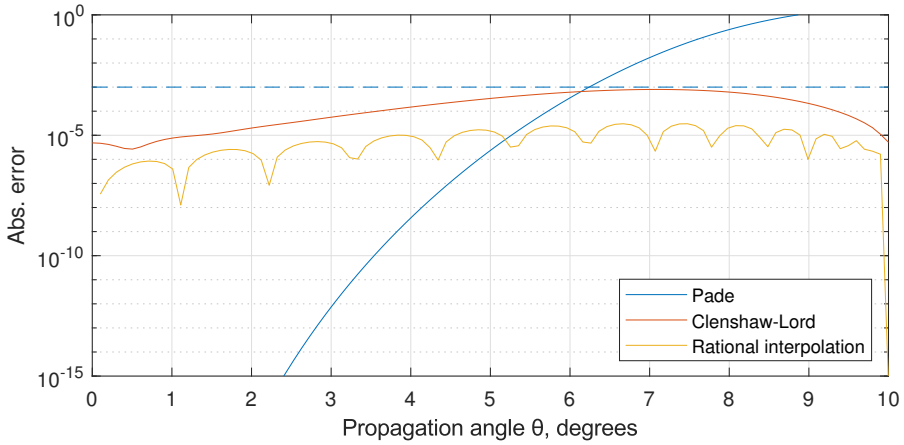

Fig. 3. Dependence of the approximation error R on the propagation angle for the Padé approximation, Clenshaw-Lord approximation, and rational interpolation in the Chebyshev roots. In all cases $\Delta x = 200\lambda$, rational approximation order is [7/7].

4 Numerical results and discussion

This section presents the results of numerical simulation obtained by the proposed method of rational interpolation and Padé approximation. An implementation of the rational interpolation method from the Chebfun library [1] was used. The rest of the functionality, including the step-by-step numerical scheme and transparent boundary conditions, is implemented in the Python 3 library [14] developed by the author.

4.1 Radio-wave propagation

In the first example, we consider the diffraction of the electromagnetic waves on an impenetrable wedge located on a perfectly conductive surface. A transparent boundary condition is established at the upper boundary of the computational domain. Problems with such geometry arise when computing the tropospheric radio-wave propagation over irregular terrain [13]. The Gaussian horizontally polarized antenna [13] is located at an altitude of 150 m above the surface and emits a harmonic signal at a frequency of 3 GHz. A 150 m high wedge is located at a distance of 3 km from the source of radiation. The wedge is modeled

ICCS Camera Ready Version 2021
To cite this paper please use the final published version:
DOI: 10.1007/978-3-030-77961-0_35

by a staircase approximation. The results obtained by the Padé approximation method and the proposed method are shown in Fig. 4 and 5. It is clearly seen that for the selected longitudinal grid step $\Delta x = 25\lambda$, the proposed method yields a correct result with an approximation order of [4/5]. At the same time, to achieve the same accuracy using the Padé approximation with the same grid size, the order of [10/11] is required. Using the order of [4/5] for the Padé approximation leads to incorrect results in the diffraction zone behind the obstacle at large propagation angles. Thus, in this example, the proposed method is more than twice as fast as the Padé approximation. The dependence of the approximation error on the propagation angle, depicted in Fig. 6, confirms these conclusions.

It should be noted that the transparent boundary condition [17, 9] originally developed for Padé approximations also works correctly for the proposed numerical scheme. However, this experimental observation requires further mathematical analysis.

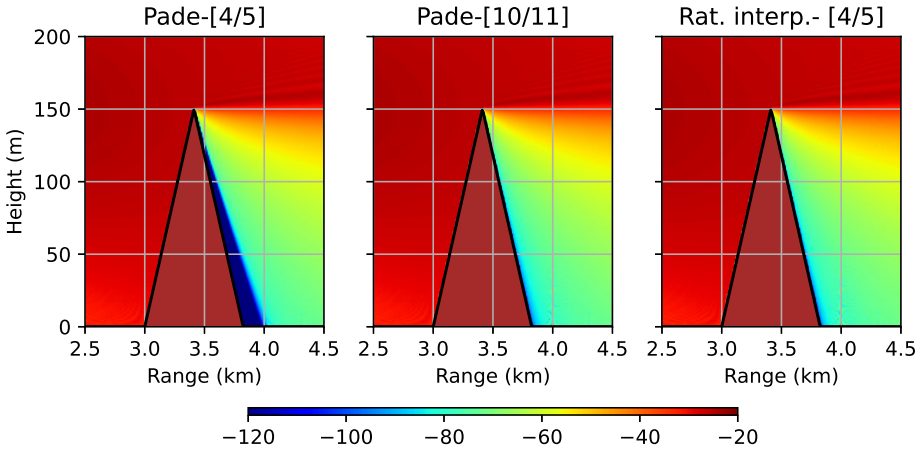

Fig. 4. Diffraction on the impenetrable wedge. Spatial distribution of the field amplitude ($20 \log |\psi(x, z)|$).In all examples $\Delta x = 25\lambda$, $\Delta z = 0.25\lambda$.

4.2 Propagation in a shallow water

In the following example, we will consider diffraction on a permeable wedge located on a permeable surface. Similar problems arise when calculating the acoustic pressure field in an inhomogeneous underwater environment. The source of 50 Hz acoustic waves is located at a depth of 50 m. The upper surface between water and air is considered smooth. The wedge and the surface on which it is located are modeled by spatial variations of the refractive index n. The field is calculated simultaneously in water and sediment, and a transparent bound-

ICCS Camera Ready Version 2021
To cite this paper please use the final published version:
DOI: 10.1007/978-3-030-77961-0_35

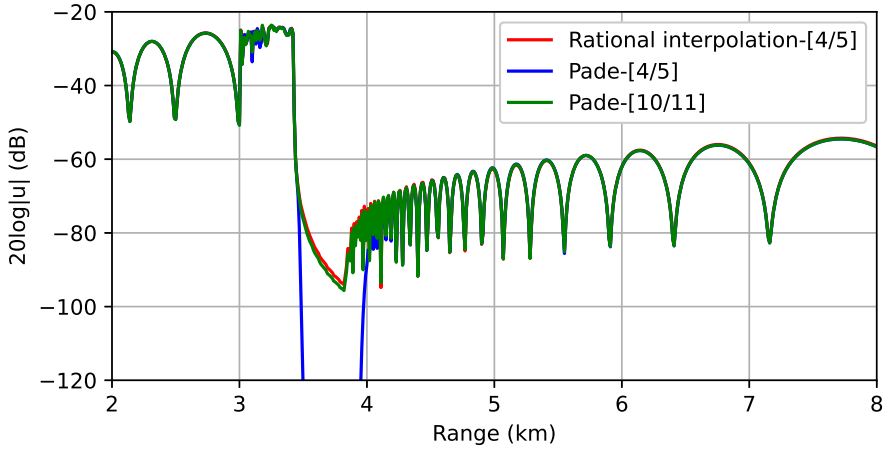

Fig. 5. Diffraction on the impenetrable wedge. Distribution of the field amplitude ($20 \log |\psi(x, z)|$) at the height of 5 m.

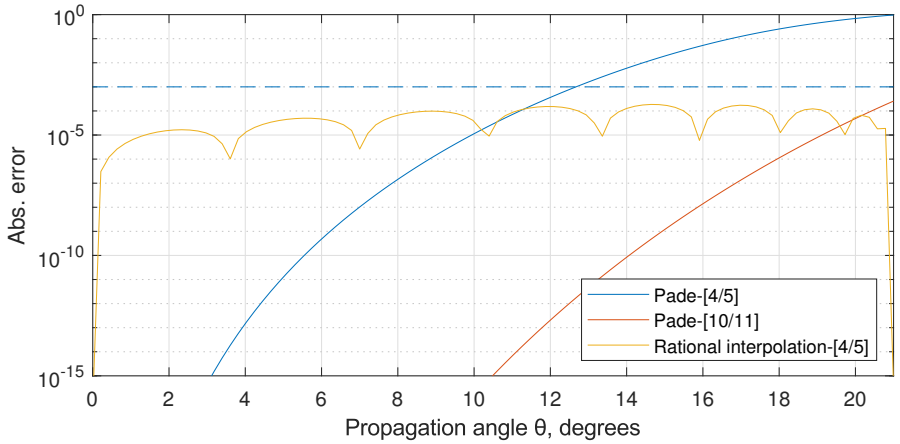

Fig. 6. Diffraction on the impenetrable wedge. Dependence of the approximation error on the propagation angle for the Padé approximation and rational interpolation, $\Delta x = 25\lambda$.

ICCS Camera Ready Version 2021
To cite this paper please use the final published version:
DOI: 10.1007/978-3-030-77961-0_35

ary condition is set at the lower boundary. The refractive index in this case is expressed as follows

$$n^2(x,z) = \left(\frac{c_0}{c(x,z)}\right)^2,$$

where $c(x,z)$ is the sound speed, $c_0 = 1500$ m/s is the reference sound speed. Constant c_0 can be chosen arbitrary, based on the fact that the wave number in this case is expressed as $k_0 = 2\pi f/c_0$. In this example, the sound speed in the water is 1500 m/s, in the sediment and inside the wedge is 1700 m/s. Additional damping of 0.5 dB per wavelength is also posed inside the sediment and wedge. For the sake of simplicity, we do not consider variations of the density in this paper, although this should be done in the future works. For the peculiarities of the mathematical formulation of computational hydroacoustics problems, we refer the reader to [6].

The results of the numerical simulation are shown in Fig. 7 and 8. The proposed scheme requires the use of the approximation order of [2/3] when $\Delta x = 6\lambda$, $\Delta z = 0.03\lambda$, while the split-step Padé method for the same computational grid requires the order of [5/6], that is, twice the computational cost. The approximation was based on the segment $\xi \in [-0.23, 0]$. The dependence of the approximation error on ξ is shown in Fig. 9.

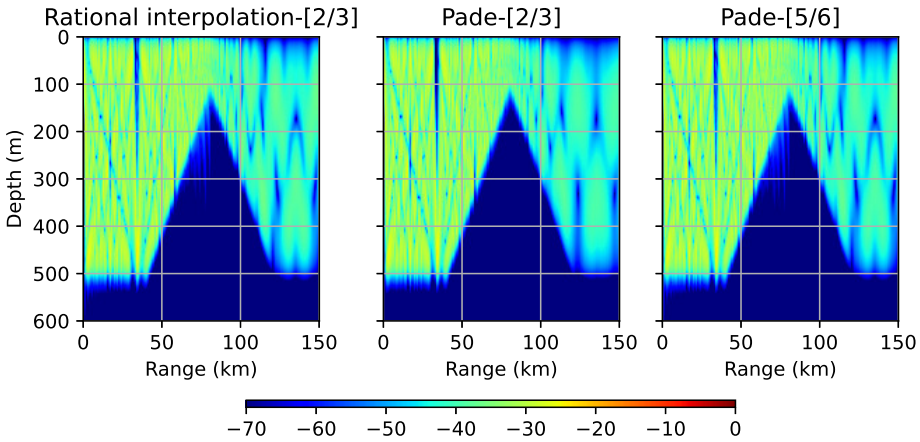

Fig. 7. Diffraction by the penetrable wedge. Spatial distribution of the field amplitude ($20 \log |\psi(x,z)|$). In all examples $\Delta x = 6\lambda$, $\Delta z = 0.03\lambda$.

4.3 Analysis of the computational grid density

In the last example, we demonstrate how the required density of the computational grid changes with increasing the maximum propagation angle θ_{max} for the

ICCS Camera Ready Version 2021
To cite this paper please use the final published version:
DOI: 10.1007/978-3-030-77961-0_35

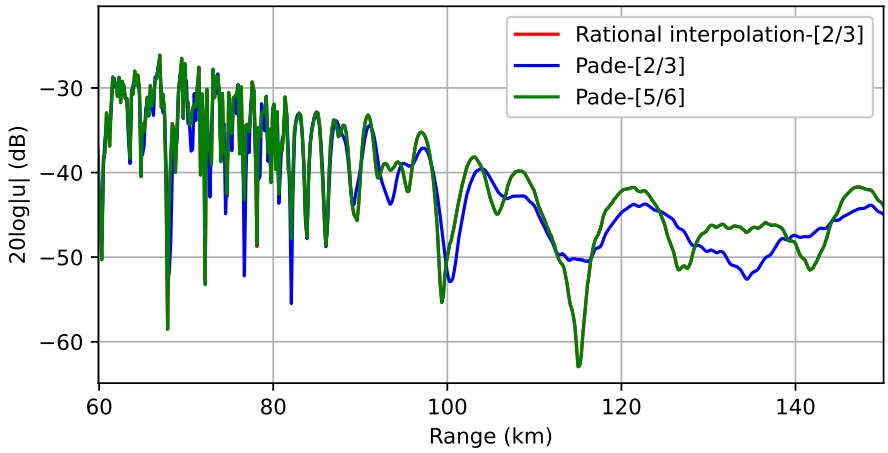

Fig. 8. Diffraction by the penetrable wedge. Distribution of the field amplitude ($20 \log |\psi(x, z)|$) at the depth of 50 m. The difference between the rational interpolation of the order of [2/3] and the Padé approximation of the order of [5/6] is not distinguishable.

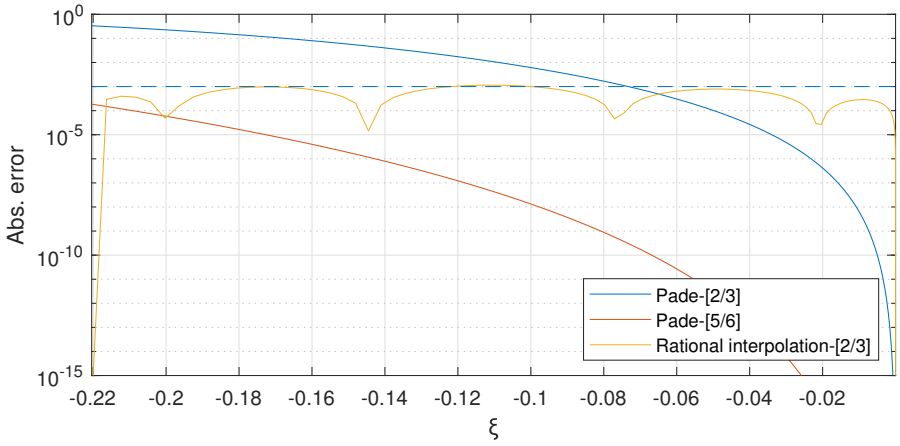

Fig. 9. Diffraction by the penetrable wedge. Dependence of the approximation error on ξ for Padé approximation and rational interpolation, $\Delta x = 6\lambda$.

ICCS Camera Ready Version 2021
To cite this paper please use the final published version:
DOI: 10.1007/978-3-030-77961-0_35

Padé approximation and the proposed method. For both methods, an approximation order of [7/8] is used. We require that at a distance of $x_{max} = 10^5\lambda$ from the source, an absolute error should not exceed $tol = 10^{-3}$. Than, following [16], we can compute the optimal value of Δx by solving the following minimization problem

$$n_x = \frac{x_{max}}{\Delta x} \to \min$$

under condition

$$\max_{\xi \in [-\sin^2 \theta_{max}, 0]} R(\xi, a_1 \dots a_p, b_1 \dots b_p, \Delta x) \cdot n_x < tol.$$

The last expression is obtained based on the assertion that the error R accumulates at each step, and the total number of steps is n_x. Table 2 shows the minimization results for the maximum propagation angles θ_{max}, equal to 3°, 10°, 20°, 45°, 60° and 80°. It can be seen that the proposed method makes it possible to use a much more sparse computational grid. Interestingly, that for propagation angles of 60° and 80° the specified algorithm could not find reasonable values of Δx for the Padé approximation method at all.

We are to keep in mind that a more rigorous mathematical error analysis of the proposed numerical scheme should be carried out in the future.

Table 2. Optimal values of the longitudinal grid step Δx for Padé approximation and rational interpolation (larger is better). The order of approximation in both cases is equal to [7/8]. '-' indicates that the target accuracy was not achieved at reasonable values of Δx.

Propagation angle θ	3°	10°	20°	45°	60°	80°
optimal Δx for the Padé approximation	600λ	50λ	11λ	1.5λ	-	-
optimal Δx for the proposed method	2600λ	200λ	40λ	8λ	4λ	1.4λ

5 Conclusion

It was shown that the use of rational interpolation on the interval gives an opportunity to decrease the computational time of the numerical scheme for solving the unidirectional Helmholtz equation by 2-5 times. It was shown that the approximation of the propagation operator on the segment is more natural for the considered problem. The proposed approach does not require significant changes to the existing numerical schemas and its implementations. A significant increase in the performance of a numerical scheme can be achieved only by changing its coefficients, without increasing the density of the computational grid or the order of approximation. The relationship between the input data of the algorithm

ICCS Camera Ready Version 2021
To cite this paper please use the final published version:
DOI: 10.1007/978-3-030-77961-0_35

(variations of the refractive index and the maximum propagation angle) and the required approximation was established. This allows us to implement more accurate and reliable numerical algorithms adapted to a particular situation. It is shown that the proposed method can be effectively applied in computational hydroacoustics and tropospheric radio wave propagation.

Other rational approximations should be studied in the future works. It is also necessary to study the stability and limitations of the proposed method, although the conducted computational experiments give reason to believe that the proposed numerical scheme, as well as the split-step Padé method, is absolutely stable. In this paper, the two-dimensional propagation was considered, but the proposed method can be generalized to a more general three-dimensional case in the future works.

References

1. Chebfun (2020), https://www.chebfun.org/
2. Baker, G.A., Graves-Morris, P.: Pade approximants, vol. 59. Cambridge University Press (1996)
3. Bekker, E.V., Sewell, P., Benson, T.M., Vukovic, A.: Wide-angle alternating-direction implicit finite-difference beam propagation method. J. Light. Technol. **27**(14), 2595–2604 (2009)
4. Brookner, E., Cornely, P.R., Lok, Y.F.: Areps and temper-getting familiar with these powerful propagation software tools. In: IEEE Radar Conference. pp. 1034–1043. IEEE (2007)
5. Collins, M.D.: A split-step pade solution for the parabolic equation method. J. Acoust. Soc. Am. **93**(4), 1736–1742 (1993)
6. Collins, M.D., Siegmann, W.L.: Parabolic Wave Equations with Applications. Springer (2019)
7. Collins, M.D., Westwood, E.K.: A higher-order energy-conserving parabolic equqation for range-dependent ocean depth, sound speed, and density. J. Acoust. Soc. Am. **89**(3), 1068–1075 (1991)
8. Ehrhardt, M.: Discrete transparent boundary conditions for schrodinger-type equations for non-compactly supported initial data. Appl. Numer. Math. **58**(5), 660–673 (2008)
9. Ehrhardt, M., Zisowsky, A.: Discrete non-local boundary conditions for split-step padé approximations of the one-way helmholtz equation. J. Comput. Appl. Math. **200**(2), 471–490 (2007)
10. Fishman, L., McCoy, J.J.: Derivation and application of extended parabolic wave theories. i. the factorized helmholtz equation. J. Math. Phys. **25**(2), 285–296 (1984)
11. Huizing, A.G., Theil, A.: CARPET Version 3 (Computer-Aided Radar Performance Evaluation Tool): User's manual (2019)
12. Leontovich, M.A., Fock, V.A.: Solution of the problem of propagation of electromagnetic waves along the earth's surface by the method of parabolic equation. J. Phys. USSR **10**(1), 13–23 (1946)
13. Levy, M.F.: Parabolic Equation Methods for Electromagnetic Wave Propagation. The Institution of Electrical Engineers, UK (2000)
14. Lytaev, M.S.: Python wave proragation library (2020), https://github.com/mikelytaev/wave-propagation

ICCS Camera Ready Version 2021
To cite this paper please use the final published version:
DOI: 10.1007/978-3-030-77961-0_35

15. Lytaev, M., Borisov, E., Vladyko, A.: V2i propagation loss predictions in simplified urban environment: A two-way parabolic equation approach. Electronics **9**(12), 2011 (2020)
16. Lytaev, M.S.: Automated selection of the computational parameters for the higher-order parabolic equation numerical methods. International Conference on Computational Science and Its Applications 2020. Lecture Notes in Computer Science **12249**, 296–311 (2020)
17. Lytaev, M.S.: Nonlocal boundary conditions for split-step padé approximations of the helmholtz equation with modified refractive index. IEEE Antennas Wirel. Propag. Lett. **17**(8), 1561–1565 (2018)
18. Lytaev, M.S.: Numerov-pade scheme for the one-way helmholtz equation in tropospheric radio-wave propagation. IEEE Antennas and Wireless Propagation Letters (2020)
19. Meng, X., Sun, J., Wei, P., Xu, Y., Xu, Z.: Superwide-angle seismic migration by including the back-scattered wave through domain decomposition and biaxial parabolic approximation. Journal of Petroleum Science and Engineering (2020)
20. Ozgun, O.: Recursive two-way parabolic equation approach for modeling terrain effects in tropospheric propagation. IEEE Transactions on Antennas and Propagation **57**(9), 2706–2714 (2009)
21. Ozgun, O., Sahin, V., Erguden, M.E., Apaydin, G., Yilmaz, A.E., Kuzuoglu, M., Sevgi, L.: Petool v2. 0: Parabolic equation toolbox with evaporation duct models and real environment data. Computer Physics Communications **256**, 107454 (2020)
22. Pachón, R., Gonnet, P., Van Deun, J.: Fast and stable rational interpolation in roots of unity and chebyshev points. SIAM Journal on Numerical Analysis **50**(3), 1713–1734 (2012)
23. Permyakov, V.A., Mikhailov, M.S., Malevich, E.S.: Analysis of propagation of electromagnetic waves in difficult conditions by the parabolic equation method. IEEE Transactions on Antennas and Propagation **67**(4), 2167–2175 (2019)
24. Porter, M.: Ocean acoustics library (2020), https://oalib-acoustics.org/, https://oalib-acoustics.org/
25. Samarskii, A.A., Mikhailov, A.P.: Principles of mathematical modelling: Ideas, methods, examples. Taylor and Francis (2002)
26. Sanders, W.M., Collins, M.D.: Nonuniform depth grids in parabolic equation solutions. J. Acoust. Soc. Am. **133**(4), 1953–1958 (2013)
27. Schmidt, F., Friese, T., Yevick, D.: Transparent boundary conditions for split-step pade approximations of the one-way helmholtz equation. Journal of Computational Physics **170**(2), 696–719 (2001)
28. Schwendt, M., Pötz, W.: Transparent boundary conditions for higher-order finite-difference schemes of the schrödinger equation in (1+ 1) d. Computer Physics Communications **250** (2020)
29. Taylor, M.: Pseudodifferential operators and nonlinear PDE, vol. 100. Springer Science & Business Media (2012)
30. Vavilov, S.A., Lytaev, M.S.: Modeling equation for multiple knife-edge diffraction. IEEE Transactions on Antennas and Propagation **68**(5), 3869–3877 (2020)

ICCS Camera Ready Version 2021
To cite this paper please use the final published version:
DOI: 10.1007/978-3-030-77961-0_35